Intricate behavior of winter pollution in Hanoi over the 2006–2020 semi-climatic period

Bao Anh Phung Ngoc, Elsa Dieudonné, Hervé Delbarre, Karine Deboudt, Song-Tung Nguyen, Van-Hai Bui, Duc-Minh Vu, Huyen-Thu Nguyen-Thi

Version of Record: https://www.sciencedirect.com/science/article/pii/S135223102300095X
Manuscript_3f902866a93f45c3d26a60db3fe770b0

Intricate behavior of winter pollution in Hanoi over the 2006 - 2020 semi-climatic period

Bao-Anh Phung-Ngoc[a,b], Elsa Dieudonné[a], Hervé Delbarre[a], Karine Deboudt[a], Song-Tung Nguyen[b], Van-Hai Bui[c], Duc-Minh Vu[d], Huyen-Thu Nguyen-Thi[b]

[a]*Laboratoire de Physique et Chimie de l'Atmosphère (LPCA), Université du Littoral Côte d'Opale, Dunkerque, France.*

[b]*Institute of Human Geography, Vietnam Academy of Social Science, Hanoi, Vietnam.*

[c]*Le Quy Don Technical University, Hanoi, Vietnam.*

[d]*Georgia State University, United States.*

*Corresponding author: Bao-Anh Phung-Ngoc

E-mail address: anh-bao.phung-ngoc@univ-littoral.fr

Abstract: During the winter period (October to March), air quality in northern Vietnam is strongly impacted by the northeast monsoon cycles, that create periodic changes in the air masses pathways and the meteorological conditions. In this work, an original approach is proposed to identify the main sources contributing to the degradation of air quality in Hanoi and quantify the share of local and imported pollution under the influence of the northeast monsoon. Firstly, semi-climatic trends in particle emissions in East Asia and mainland Southeast Asia were studied using outputs from the NAAPS model, that assimilates space-borne Aerosol Optical Depth (AOD) observations. From winter 2006/07 to winter 2010/11, the pollution plumes were most frequently located over the Indochina Peninsula, and the smoke partial AOD showed biomass burning activities (natural and anthropogenic) to be responsible. From winter 2011/12 to winter 2019/20 however, the pollution plumes were mostly observed over eastern China and to a lesser extent, Northern Vietnam, and the sulfate partial AOD indicated they came from coal-based industrial activities. Secondly, the impact of the northeast monsoon on the air masses origin was studied using HYSPLIT back-trajectories with clustering over the 14 winter periods. During regular winters, northeastern air masses predominated, which can bring pollution from eastern China and the industrial region surrounding Hanoi (Red River Delta). However, the existence of El Niño perturbed the air masses trajectories during three winters (2014/15, 2015/16 and 2018/19), bringing more western air masses and thus, causing a temporary decrease of the sulfate AOD and simultaneous increase of the smoke AOD over Hanoi. Thirdly, a method to classify the winter days and highlight the influence of cold surges on $PM_{2.5}$ variability was built, relying only on Hanoi local wind and NAAPS AOD value. This

classification allowed to estimate that long-range transport from China during the onset of cold surges caused an average increase of around 30 % of the $PM_{2.5}$ level in Hanoi. Additionally, the contribution of local pollution to the most severe pollution episodes, occurring during the persistence of cold surges, was estimated to be around 40 % of the average $PM_{2.5}$.

Keywords: Air pollution; AOD; cold surge; meteorology; $PM_{2.5}$

Abbreviations:

AOD:	Aerosol Optical Depth	OC:	Other Conditions
AERONET:	Aerosol Robotic Network	PM:	Particulate Matter
HYSPLIT:	Hybrid Single-Particle Lagrangian Integrated Trajectory	SC:	Stagnant Condition
LRT:	Long-range transport	TTPs:	Thermal Power Plants
NAAPS:	U.S. Navy Aerosol Analysis and Prediction System	WD:	Wind Direction
NEHA:	Northeast high AOD	WS:	Wind Speed
NELA:	Northeast low AOD	WRF/CMAQ:	Weather Research and Forecasting/Community Multiscale Air Quality Modeling

1. Introduction

Over the last decade, severe pollution episodes with high level of PM tended to be observed frequently over the Red River Delta (RRD) plain, Northern Vietnam, especially during the winter period (October to March) during which the Northeast monsoon is predominant. Due to rapid economic development, urbanization, and industrialization, the RRD has long been recognized as one of the most polluted regions in Vietnam (Bac and Hien, 2009; Le et al., 2020). In addition, most of the key industrial zones, along with most of the thermal power plants (TPPs) of Northern Vietnam are concentrated over the RRD region (Huy and Kim Oanh, 2017). The consumption of large amounts of coal and fossil fuels in these TPPs in order to meet the growing electricity demand over the last decade released an enormous amount of gaseous and particulates compounds. Industrial zones and TPPs are major sources of local pollution and regional transport, and are partly responsible for the degradation of air quality in the RRD. However, local pollution and regional transport may not be the only sources as the RRD area has been

stated as a potential receptor for transboundary long-range transport (LRT) from East-Asia under the impact of the Northeast monsoon during the winter period. Concerning the daily variability in this period, an increase in air pollutant levels over the couple of days that follow a cold surge was observed in areas located downstream of China such as Taiwan, Malaysia and Northern Vietnam (Ashfold et al., 2017; Chen et al., 2014; Cohen et al., 2010a; Junker et al., 2009).

Within RRD area, Hanoi, Vietnam's capital has suffered bouts of repeated and continuous air pollution with high ambient levels of particulate matter in the last decades. The high levels of $PM_{2.5}$ observed in Hanoi, in particular, often exceed the national ambient air quality standards (daily $PM_{2.5} > 50$ μg m^{-3}) during the winter period. In fact, many studies on the air environment have been carried out with the aim of giving a picture of the current status of the air environment in Hanoi. Nevertheless, most of these studies were limited to a short-term period of investigation (from a month to a few months) and there was no analysis bearing on the whole winter period, nor on long-term variations of ambient pollutants' concentrations in Hanoi. For example, Nguyen et al. (2020) used the Weather Research and Forecasting/Community Multiscale Air Quality Modeling (WRF/CMAQ) system to simulate the contribution of different sources to the total $PM_{2.5}$ concentration in December 2010. Although, they reported that local and non-local sources accounted respectively for 57% and 43% during high pollution events, and 42% and 58% during lower pollution periods, this conclusion stood only for one month of the winter period. On the other hand, some studies have a longer study period but are based on older data from years when air pollution was not as explosive as it is nowadays. For instance, using Positive Matrix Factorization/PMF analysis, Hai and Kim Oanh. (2013) stated that the LRT was likely to represent a smaller part of the total $PM_{2.5}$ (about 27%) compared to local pollution from December 2006 to February 2007. One of the longest studies conducted by Cohen et al. (2010a, 2010b), they reported the fingerprint source and contribution of fine particles ($PM_{2.5}$) in Hanoi, however, these studies were based on measurement results from 2001 to 2008, which is a very long time compared to the current state of the air quality.

Thus, in order to evaluate the air pollution trend in Hanoi, it is imperative to obtain a detailed dataset, based on long-term and continuous observations and modeling of airborne pollutant trends and their variability. Besides, information is lacking about the inter-annual variations of air pollutants in Northern Vietnam, in relation with changes in the Northeast monsoon. This hinders the possibility to detect trends in specific emission sources, quantify the local and remote sources'

contributions, and fully understand the mechanisms of pollution events in Hanoi. To address the above-mentioned shortcomings, our goal in this study is to answer the following questions:

(i) What are the main aerosol sources region in winter in East and South-East Asia and what are their trends over the 2006 - 2020 period?

(ii) Which sources are actually susceptible to impact northern Vietnam through long-range transport, and what is the influence of the monsoon inter-annual variability on their contributions?

(iii) What is the contribution rate of the various sources to the air pollution issue in Hanoi at daily scale?

In detail, as long time series of $PM_{2.5}$ concentrations in Vietnam are lacking, AOD retrieved from U.S. Navy Aerosol Analysis and Prediction System (NAAPS) model is chosen as a proxy for $PM_{2.5}$. 14-years database of AOD from 2006 to 2020 was built up in order to identify the pollution sources areas and their inter-annual evolution over East Asia and Southeast Asia, allowing question (i) to be addressed. In addition, a combination was made between long-term AOD database and backward trajectories conducted from the Hybrid Single Particle Lagrangian Integrated Trajectory (HYSPLIT) model in order to analyze long-term AOD trends and the inter-annual variability of the Northeast monsoon under the influence of El-Niño events. From this, the potential emission sources impacting Hanoi from question (ii) will be assessed, with the goal to explore the adverse effects of meteorological conditions on air quality in Hanoi. At last, to solve the question (iii), we will finally propose a systematic procedure for identifying the impact of the cold intrusions on the air quality in Hanoi at a daily scale, by fully combining backward trajectories, NAAPS-AOD data, in-situ $PM_{2.5}$ and weather observations.

2. Material and Methods

2.1 Study area and in-situ observations

Hanoi is located on the plain of the RRD (Fig. 1 a - b) which is the most densely populated region of Northern Vietnam. Hanoi, during the winter, often annually receives 10 to 15 Northeast monsoons taking place from October to March of next year, not only directly affecting to the weather conditions of Hanoi but also causing the change in air quality. For investigating potential sources impacting air quality in Hanoi, pollution sources are classified into local pollution, regional transport and LRT corresponding respectively to sources within Hanoi (transport, construction, cooking, etc.),

sources within a radius below 200 km from Hanoi and above 200 km, respectively. The location of industrial zones and thermal power plants in the RRD is shown in Figure 1(c); these sources, located not far away from Hanoi, are expected to be the main contributors for the regional sources. In more details, the coal-based electricity production in Vietnam grew from 11.9 billion kWh in 2008 to nearly tenfold at 119.1 billion kWh in 2019. Additionally, the of number of coal-fired TPPs across Vietnam increased from 6 to 29 between 2009 and 2019 in order to meet the national electricity's growing (Le et al., 2021). The nearest coal-based power plant is located only 50 km away from Hanoi and has been recorded as the highest SO_2 emitter among TTPs in Northern Vietnam. Last but not least, LRT is considered as an atmospheric transport over distance larger than 200 km, which mainly comes from transboundary sources in China or in other countries of the Indochina Peninsula. Regarding in-situ observations over Hanoi, this study relies on local meteorological data obtained from the Vietnam Meteorological and Hydrological Administration and $PM_{2.5}$ data from the monitoring station installed at the US Embassy have been analyzed. The meteorological data cover the full study period (2006 - 2021) but the $PM_{2.5}$ time series only starts in December 2015 only.

2.2. Northeast monsoon definition

Northeast monsoon, which also named as cold surge or cold intrusions, has been variously defined according the research scope. For example, Hien et al., 2011 studied it by coupling of synoptical weather patterns with terrain effect according to temperature, while Chen et al., 2002 who identify a cold surge event by the following changes of meteorology within 24 ~ 48 h: (a) surface pressure increases more than 5 mb, (b) surface temperature drops higher than 4°C, (c) surface prevailing wind is stronger than 3 m s^{-1}. Previous observations at Hanoi (Phung Ngoc et al., 2021) demonstrated that the changes in local wind were very well correlated with the abrupt drop in temperature and relative humidity occurring at cold surge onsets. Thus, in the present study, all cold surges are selected when the daily temperature drops by more than 4°C and the prevailing wind is northerly/northeasterly (directions in the 0° to 90° range) with a wind speed stronger than 3.1 m s^{-1}.

2.3 Aerosol Optical Depth (AOD) data

NAAPS is an operational aerosol transport model produced by the U.S Navy that produces forecasts of three-dimensional aerosol concentrations on a global scale, combining the current satellite data with global aerosol simulations (https://www.nrlmry.navy.mil/aerosol/). This model

operates with a 6-hour temporal resolution, a 1° × 1° horizontal resolution, 25 vertical sigma-pressure levels and Navy Global Environmental Model/NAVGEM meteorological fields produced by the U.S Navy (Hogan et al., 2014). The model provides the total AOD values and their components including smoke, dust and sulfate AOD values.

With the aim of validating the AOD retrieved from NAAPS, the daily average of ground-based Level 2.0 AOD from Aerosol Robotic Network (AERONET) (http://aeronet.gsfc.nasa.gov) was extracted for the winter period (October - March) from 2010 to 2019 at Nghia-Do AERONET station (21.04°N, 105.79°E) located within Hanoi urban area, in a residential and urban area characterized by large traffic emission from a ring road and several other busy-roads. For NAAAPS model, the AOD in the pixel covering Hanoi was extracted over the same time period and daily averaged by considering only days with available AERONET observations. Finally, the 6-month winter mean AOD in Hanoi was computed from both NAAPS and AERONET data, from winter 2010/11 to winter 2018/19 (Fig. 2).

Figure 2 (a) shows that the simulated AOD is largely underestimated compared to ground-based observations, as was already found by previous studies (Chew et al., 2016; Maciszewska et al., 2010). Part of the discrepancy between the observations and the model can be explained by the difference of wavelength between AERONET (AOD at 500 nm) and NAAPS (AOD at 550 nm). Assuming an Angstrom exponent of 1, the AERONET AOD values would decrease by 10% if the wavelength correction was applied. However, it was chosen not to apply the correction in this study in order not to add an extra cause of uncertainty. The AERONET AOD values can also be higher because they are measured in the center of Hanoi, while the spatial scale of NAAPS model (1°×1°) is not fine enough to resolve such a pollution hot-spot. A third reason for discrepancies could be the difference in satellite and ground-based observations data availability. AERONET delivers a daily AOD value provided that there was at least one observation, i.e. at least one few-minute clear-sky period of a few minutes at any time during the day. On the contrary, the satellite AOD observations used to constrain NAAPS are recorded at precise times of the day (around 11 a.m. and 1 p.m. for the MODIS instruments) so that NAAPS will not be constrained on a given day if the sky is cloudy at the times the satellites pass over. It is therefore possible to have points in the comparison corresponding to unconstrained, i.e. lesser quality model data. However, in spite the large underestimation of the AOD by NAAPS, the model accurately reproduces the AOD trend and inter-annual variability over Hanoi. Therefore,

NAAPS AOD is considered to be reliable proxy to study the evolution of particle sources in SEA and EA over 14 years (Section 3.1) and the impact of the inter-annual variations of air mass origin on air pollution in Hanoi (Section 3.2).

In order to assess the ability of NAAPS model to reproduce the day-to-day variability of the AOD, Figure 2 (b) presents the scatter plot of the NAAPS-AOD model results versus the AERONET-AOD from Hanoi station. The correlation coefficient between the model and the ground-based observations was moderate (0.66); the slope of the linear regression was far below 1 (0.52), in agreement with the large underestimation of the AOD by the model that was already pointed from Figure 2 (a), but the intercept was very small (0.08), meaning the model has no systematic bias compared to the observations. In this study, single-day NAAPS-AOD values were used in a binary way (i.e. the AOD higher or lower than the average value) in order to discriminate between days impacted or not by long-range transport. Therefore, to qualify NAAPS AOD for this purpose, the scatter plot was split into four quadrants using the mean of values of NAAPS-AOD and AERONET-AOD computed from all the coinciding data from the winters 2010/11 to 2018/19. 73 % of the points fall in the first quadrant (N1) and the third quadrant (N3), meaning they are correctly attributed to the low/high AOD category, which is a pretty good score for such a global-scale model. Therefore, NAAPS model was considered to be good enough to detect LRT pollution in this study (Section 3.3 and 3.4).

2.4 HYSPLIT data

The HYSPLIT model (Stein et al., 2015) has been used for generating air mass backward trajectories and highlight potential sources for transported emissions into Hanoi. The Global Data Assimilation System/GDAS1 data with a 1° × 1° resolution was selected as meteorological input to calculate 4-days backward trajectories for every day during the winter period from winter 2006/07 to winter 2019/20. All backward trajectories were then grouped into 6 clusters by the HYSPLIT integrated tool, which minimizes the total spatial variance using k-means clustering.

In a similar way with other backward-trajectory models, HYSPLIT has some computational uncertainties with the horizontal uncertainty of the trajectory location being around 10 to 20% (Draxler and Hess, 1998). Moreover, the uncertainty on the coordinates of trajectories computed from wind fields was as assessed to be of the order of 20% of the travel distance (Stohl, 1998). In

order to enhance the accuracy of this model, the use of a large number of trajectories can be combined in a statistical analysis (Cabello et al., 2008). Thus, for this study, the cluster analysis was performed on the 30,926 backward trajectories computed over the 14 winter periods. In addition, the time-step has been kept short (one hour) in spite of the number of trajectories to compute, in order to improve the model accuracy.

2.5 Classification of winter days in Hanoi

The classification method is illustrated in Figure 3 and used for identifying the contribution of local pollution, regional transport and LRT on air quality in Hanoi during the winter period. The proposed method is followed as below:

(i) Wind speed (WS): This first parameter is used to discriminate between days that correspond to stagnant condition and strong wind conditions. WS higher than the average value in Hanoi (3.1 m/s) is used as a threshold for detecting strong wind episodes. The remaining cases are assigned to “Stagnant conditions” days or SC.

(ii) Wind direction (WD): During strong wind days, WD is a key parameter for determining the days under monsoon’s impact. As a result, the WD within 0^o and 90^o is used as the indicator of Northeast monsoon’s days. The remaining cases are assigned to “Other conditions” or OC.

(iii) Sulfate AOD: Among the days under the impact of the Northeast monsoon onset, sulfate AOD from NAAPs model is used as a tracer to discriminate the days during which a large-scale pollution plume from China was present. As the meteorological conditions were similar during all the onset days, the local and regional emissions and their transport can be considered to be the same. And the emissions can also be considered to be similar, so that the only difference is the presence, or absence, of a large-scale pollution plume from mainland China. When a plume is present (or respectively absent), the sulfate AOD from NAAPS is higher (or respectively lower). The average sulfate AOD value of 0.63 is used as a threshold for determining how the Northeast monsoon affects Hanoi's air quality. The days which are accompanied by relatively high sulfate AOD values (> 0.63), are classified as “Northeast high AOD” (NEHA) and considered to correspond to cases when the large-scale plume from China is present. On the contrary, the days with lower values of sulfate AOD (< 0.63) are classified as "Northeast low AOD" (NELA) and considered to represent cases when no large-scale plume is present.

3. Results

3.1 Spatial and temporal distribution of AOD in East Asia

Figure 4 shows the spatial distribution of the 6-months averaged-total AOD retrieved from the NAAPS model during the winter period in EA and mainland SEA from winter period 2006/07 to period 2019/20. With the aim of investigating the characteristics of AOD sources for the studied area, not only the total AOD but also its components (sulfate, smoke and dust partial AOD) were further analyzed. The dust partial AOD distribution did not show any interesting feature over the study area, but the smoke and sulfate partial AOD maps are presented in Figures A.1 and A.2 respectively. By looking at the maps, the 14-years study period can be divided into 2 stages. During the first stage, from the winter period 2006/07 to period 2010/11 (Fig. 4a – e, green square), high value of total AOD (> 0.7) were observed frequently over the Indochina Peninsula regions (northern Laos, near the Myanmar boarder, northern Thailand and Northern Vietnam). According to previous studies, a dominant influence of biomass burning activities originating from both natural (forest fires) and anthropogenic sources (agriculture) in this region was demonstrated (Nguyen et al., 2021; Reid et al., 2013). This point is confirmed by the fact that high smoke partial AOD values (> 0.7) were retrieved by NAAPS model over the same regions of the Indochina Peninsula region (Fig. A.1a - f).

Over the northern part of inland China, moderate AOD values (from 0.4 to 0.6) were retrieved during the first stage (Fig. 4a - e, purple square). However, during the second stage of the study period, from winter 2011/12 to winter 2019/20, the AOD values observed over the North China Plain, Eastern China, and Sichuan Basin areas started to rise steeply (Fig. 4f - n). High (> 0.7) and even very high (> 1.0) AOD values were observed over inland China, especially during the last four winter periods (Fig. 4k - n, purple square). The high AOD values observed over these areas are consistent with results from previous studies about the spatial distribution of AOD in the interior of China (Kuerban et al., 2020; Li, 2020). These regions of China are known as dense industrial regions including numerous refineries, factories and thermal power plants (Cohen et al., 2010b; Pu et al., 2015). Indeed, Figure A.2(f - n) show that the high values of total AOD observed over inland China mainly consisted of sulfate AOD, indicating that these aerosols were formed in an environment rich in SO_2, a pollutant mainly emitted by coal-based industrial activities.

Besides the interior of China, high values of total AOD started to be observed in the RRD since winter 2016/17 (Fig. 4k - n, blue square) that were also composed mainly of sulfate AOD (Fig. A.2k - n) following the rapid development of industrial activities in the RRD. Therefore, there were three main aerosol sources in East Asia that may have impacted air quality in Hanoi during the study period: first, biomass burning sources in the Indochina Peninsula from the winter period 2006/07 to period 2011/12, then industrial sources in inland China since the period 2011/12 and finally, closer industrial sources in the RRD from the period 2016/17.

3.2 Origin of air masses ending at Hanoi from 2007 - 2020

The large number of backward trajectories calculated for the winter period (6 months) with the HYSPLIT model can cause overlapping issues (Fig. A.3), leading to difficulty in determining the exact direction of air masses. In order to investigate the aerosol sources that actually impacted the Hanoi's air quality, the clusters analysis method was used. Figure 5 presents the mean back-trajectory for each of the 6 clusters that were computed from all the 96-hour back-trajectories ending at 100m a.g.l in Hanoi every hour during 14-winters from 2006/07 to 2019/20.

In agreement with past studies (Ly et al., 2021; Phung Ngoc et al., 2021), the cluster analysis in this study shows that the main air masses arriving in Hanoi during the winter period originated from the northeast direction, with cluster C1, C2 and C3 accounting for approximately 70% of the total number of back-trajectories. These air masses were divided into three groups: Clusters C3 come from Siberia and passed directly through inland China, bringing dry and cold air to Northern Vietnam. In contrast, the air masses from cluster C2 also originated from Siberia but travelled a longer pathway over the East Sea before reaching Northern Vietnam via the Gulf of Tonkin. These air masses carry humid and cold air and sometimes bring heavy rain to the North of Vietnam (Minh, 2007). Cluster C2 occurs when the Siberian high-pressure system shifts towards the East. In general, the altitude of all northeast clusters was lower than 2000 m (Fig. 5b). Previous studies about the depth of boundary layer in China and Vietnam found heights between 900 and 1500 m in winter (Leng et al., 2016; Miao et al., 2018; Phung Ngoc et al., 2021) so that these northeast air masses may travel within the boundary layer and catch the pollutants emitted along the trajectory. At last, C1 clusters also originated from South China but over a much a shorter distance, due to lower wind speed. These trajectories probably occur during prolonged anticyclonic episodes, which will be further explained in the next section.

Furthermore, Figure 5(a) shows that these northeast air masses passed over the densely populated and densely industrialized areas mentioned in section 3.1. Therefore, these clusters are likely to be associated with a transfer of the pollutants accumulated above the interior of China and the Red River Delta plain toward Hanoi.

Otherwise, the cluster C4 corresponds to southeast air masses originating from the South China Sea (Fig. 5a), which were considered as clean flow in this study and represented ~15 % of the total number of back-trajectories. At last, there were also some westerly air masses coming from North of India and the Bengal Bay (clusters C5 and C6) that accounted for ~14 % of the total. The latter air masses moved from a higher altitude than the northeast air masses, especially cluster C6 that come from an approximate altitude of 5000 m (Fig. 5b). This can be explained by the geographical conditions, with mountains being on these cluster trajectories. Usually, westerly flows are recorded frequently only after the southwest monsoon starts, at the end of March or beginning of April (Co et al., 2014). The appearance of clusters C5 and C6 during the winter period might therefore correspond to anomalous activities of the air masses in Northern Vietnam. As a matter of fact, biomass burning aerosols from Indochina have been proven to occasionally impact air quality in the Northern Vietnam and South China during the studied period (Huang et al., 2013). However, the western air masses were not dominant during the studied period since they only account for around one seventh of the total (Fig. 5a).

3.3 Analysis of AOD variability with sources and transport pathway

With the aim of highlighting the relationship between the semi-climatic oscillations and the air quality in Hanoi, the frequency of occurrence of clusters was computed for each of the 14 winters, along with the winter-averaged AOD values from the NAAPS model, for the pixel covering Hanoi. The time series of the clusters frequency and AOD values (total AOD along with the smoke, sulfate and dust partial AODs) are presented in Figure 6. The air masses originating from the northeast direction (clusters C1, C2 and C3) were always dominant over southeast and western air masses, but their frequency varied widely from year to year, between 44 and 88 %. The western air masses (cluster C5 and C6) experienced even wider year-to-year variation, oscillating between 3 and 39 %, while the contribution of the southeast air masses (cluster C4) was more regular (10 to 18 %). In detail, clearly larger contribution of western clusters was observed during two winters 2014/15 and 2015/16 (Fig. 5). Some studies indicate that the high-pressure system in Siberia was weakened during these winters along with the

existence of a strong El-Nino episode, which led to less cold air being transported from Siberia toward the south during these years (Chang et al., 2016; Zhao et al., 2018). Moreover, the same studies indicate that cyclonic anomalies near the Bay of Bengal were produced, then transported warm and moist air from the Bay of Bengal to the continental regions of South China and the Indochina Peninsula. Therefore, it appears that western clusters tended to be more frequent – and northeastern clusters less frequent – in winter periods occurring during strong El Niño episodes.

The winter-averaged total AOD varied widely, between 0.19 and 0.79, with the strongest values being observed during the last three winters (2017/18 and onwards, Fig. 6). The dust AOD can vary widely in relative terms (from 0.04 to 0.12), but it always represented a very minor part of the total AOD and showed no remarkable trend over the study period. The smoke partial AOD experienced a general decrease over the study period, from 0.52 during winter 2006/07 to 0.10 or less during the last four winters. Conversely, the sulfate partial AOD went through a very strong increase, from 0.04 during winter 2006/07 to 0.68 during the last two winters. Consequently, the smoke partial AOD was dominant until winter 2012/13, while the sulfate partial AOD became dominant from winter 2013/14 and onwards, which correspond approximately to stage one and stage two defined in the time series of AOD maps from Figure 4. It should be noticed, however, that the above-mentioned trends in sulfate and smoke partial AODs were interrupted during the winters 2014/15 and 2015/16; during those winters, the sulfate AOD suddenly fell down and the smoke AOD increased simultaneously. This interruption could be explained by the perturbation of air masses trajectories induced by El-Nino: with the increased frequency of western air masses, Hanoi received more smoke originating from biomass burning activities in the Indochina Peninsula. In contrast, the frequency of the northeast clusters was reduced, corresponding to a decrease in the LRT and RT of sulfate particles from China and the Red River Delta, respectively. The very high sulfate AOD values and very low smoke AOD values observed during the last three winters (2017/18 and onwards), can be explained firstly by the rapid growth of industrial development in the area. However, meteorology was also competing with emissions for explaining the rapid increase in sulfate partial AOD from winter 2013/14 onwards. The variation of AOD values and its components seem to be changed by the particularly high contribution of northeast air masses prevailing during these winters (78 to 87 %) and by the particularly low contribution of western air masses (only 3 to 4 %). This indicates

that the dominant air masses (e.g. Northeast monsoon) dramatically affects the type of aerosol as well as aerosol load over Hanoi during the winter period by the effect of RT and LRT.

The growth of sulfur compounds emissions in the RRD and the China mainland likely played a role too. As mentioned in Section 2.1, the number of coal-fired TTPs in Vietnam has increased from 6 to 29 between 2009 and 2019. Specifically, 10 TPPs were located in the RRD, with the nearest one and largest SO_2 emitter being located only 50 km away from Hanoi. The rise of sulfate AOD may therefore also result from this increase in local pollution and regional transport following the rapid industrialization and coal consumption growth in Hanoi and its surrounding areas. Regarding China's coal consumption, from 2004 to 2017, it experienced significant variability, from a rapid increase (2004 - 2013) with an annual growth rate of 8.3 % to a slowly falling stage after 2014 (Yuan, 2018). Furthermore, coal-based electricity production still accounts for 60 % of total energy consumption in China in 2015 (Cui et al., 2021). Previous studies indicated that secondary sulfate-rich compounds (products of the oxidation of SO_2) from coal-fired power stations or industrial emissions could be transported to the downwind regions including Vietnam by LRT process, and subsequently transformed into an aerosol. Furthermore, sulfate was one of the most abundant species among all water-soluble ions in aerosols found in China during winter (Chuang et al., 2018; Ding et al., 2019). In the end, the growth of sulfate AOD since the winter 2013/14 results from a combination between more sulfur compounds emissions in the RRD and in China and more favorable wind paths for regional transport and LRT of these pollutants towards Hanoi. The sulfate partial AOD, therefore, that was shown to associate to the share of northeastern air masses, was used in the rest of the study as a tracer of RT and LRT in order to investigate the impact of the Northeast monsoon on air quality in Hanoi.

3.4 Diurnal variation of $PM_{2.5}$ in Hanoi under the impact of cold surges

Table 1 displays the mean of meteorological parameters and of $PM_{2.5}$ during the last four winter periods in Hanoi, for which the $PM_{2.5}$ data were available. There was no significant change of temperature, humidity and wind speed over these winter periods. Regarding WD, the predominance was southeast, which accounted for half of the total frequency of WD. In addition, the contribution of northeast winds varied from 27.4 to 34.6 %. In the case of sulfate AOD, the trend was still upward in winter 2016/17 during which a lower value (0.46 ± 0.27) was observed. For the last three years, the mean sulfate AOD value was pretty constant.

Each day from the 4 winters was classified among three stages owing to the Northeast monsoon effect (Fig. A.4). To better introduce these stages, a zoom was made on a typical winter period, from December 19th 2019 to February 05th 2020 (Fig. 7). The onset of cold surges was ascribed to phase 1 (red areas from December 19th, 26th, January 11th, 16th, 26th and February 06th on Figure 7). This phase lasted generally between 2 and 4 days, however, the characteristic changes occur during the first two days of phase 1. In detail, the daily temperature decreased rapidly (≥ 4°C) (Fig. 7a), combined with a sharp increase in WS (≥ 3.1 m s^{-1}) (Fig. 7d). Due to the rise in WS, dispersion and transport of local pollution were greatly enhanced, resulting in a relatively low-level of $PM_{2.5}$ (< 50 μg m^{-3}) throughout phases 1 (Fig. 7g). The sulfate AOD witnessed a general increase upon the cold air arrival during the four winter periods (Fig. 7g), possibly due to LRT from the China in elevated aerosol layers that did not impact ground-level concentrations. Therefore, there was no major correlation between sulfate AOD and ground-based $PM_{2.5}$ during phases 1.

Phase 2 referred to the period during which the high-pressure system persisted and engulfed Northern Vietnam, which lasted commonly from 5 to 8 days (grey areas in Fig. 7d, from December 23th, 28th, January 12th, 20th and February 28th). The surface air pressure tended to rise in phase 1 due to the effect of the anticyclone, then it started decrease in phase 2, as shown in Figure 7(b). Moreover, wind speeds were also significantly attenuated because of the impact of the high-pressure system, resulting in stagnant conditions and severe pollution episodes: as the $PM_{2.5}$ level rose (Fig. 7g), the visibility decreased (Fig. 7f). Unlike phase 1, the variations of $PM_{2.5}$ and sulfate AOD seemed to be more correlated during phase 2 (Fig. 7g), suggesting that aerosols in the boundary layer represented most of the AOD. At the end of phase 2, there were two possible scenarios: (i) a new cold surge was observed, resulting in a new circulation with phases 1 and 2 repeated, or (ii) southeast trade winds from the ocean arrived, bringing warmer and more humid air (Fig. 7a and c, from January 02nd, 15th, 23rd and February 03rd). This last case not influenced by cold surge, was called phase 3 and was associated with low level of $PM_{2.5}$ and sulfate AOD values (Fig. 7g) as it brought clean marine over Hanoi; it lasted normally from 4 to 6 days. In addition to phase 2, the pressure in phase 3 continued to decrease significantly (Fig. 7b).

Table 2 displays the key aspects of meteorology, sulfate AOD, and ground-based $PM_{2.5}$ during each phase, computed over the whole 4 winters. As said above, phases 1 (onset of the cold

intrusions) were the coldest with an average temperature that was generally below the monthly average temperature (-2.16 ± 3.03 ^{o}C). WS values above the monthly average were observed during both phase 1 and 3 while they were clearly lower during the stagnant phase 2. $PM_{2.5}$ concentration in phases 2 (persistence of the anticyclone) was beyond the monthly mean; and phases 1 or phases 3 (trade winds episodes) showed an opposite result. Phases 3 had the lowest sulfate AOD (-0.09 ± 0.19 against ~ 0.03 for phases 1 and 2) as was expected for marine air masses. Phase 1 might seem shorter but it still represented 21 % of the winter days and occupied 34 days in average during a winter. Phase 2 was dominant and represented 55 % of the winter days, it lasted 87 cumulated days in average. Phase 3 accounted for 24 % of the days and occupied 38 days in average.

Figure 7(g) and A.4 also depicts the types of days mentioned in Figure 3, including NEHA, NELA, SC and OC. According to the classification, the NEHA (red bars) and NELA (blue bars) days were mostly seen in phase 1 as they correspond to strong wind condition with NE wind direction, which is typical for the cold surge onset. On these days, local pollution was substantially diluted while regional transport and LRT played a direct role in the formation of $PM_{2.5}$. Figure 8 presents the average $PM_{2.5}$ concentration for the different types of days and the four winters. In spite of the inter-annual variability in the overall level of $PM_{2.5}$, the relative variations of concentrations between the different types of days exhibited the same behavior during the 4 winters. The lower concentrations observed in all types of day over the winter 2018/19 can be explained by the El-Nino phenomenon that occurred during this winter. According to Wang et al., 2006, the peak in the inter-annual sea surface temperature anomalies across the South China Sea occurs during the month of February following the El-Nino onset. In February 2019, as a consequence of the anomaly, the trade winds (phase 3) were dominant, and only one weak cold surge was reported for the whole month (Fig. A.4c). Furthermore, the $PM_{2.5}$ levels were generally lower during winter of 2018/19 than during the other three winters (fig. 8 and A.4); as a result, not a single day during winter 2018/19 had $PM_{2.5}$ concentrations surpassing the national regulatory threshold.

Figure 8 also indicates that, for the four winter periods from 2016 to 2020, the average $PM_{2.5}$ concentration was higher during the high-AOD days (NEHA) by about 9 to 17 μg m^{-3} (30 to 35 %) compared to the low-AOD days (NELA). This indicates that the transported pollutants can remain at high altitude instead of mixing down to the ground, at least for some time, leading to

higher AOD value on NEHA days. In contrast, the ground-based $PM_{2.5}$ concentration were attenuated due to higher wind condition. Therefore, even though AOD is difficult to relate to ground-level concentrations, it can be used as a proxy to distinguish between air masses impacted or not by RT and LRT during the cold surges.

Besides, the SC days, which corresponding to stagnant conditions, occurred mainly during phase 2 (Fig. 7g), after the onset of cold surges. During these days, the impact of the Northeast monsoon decreased and, as less pollutants were imported from China, the formation of $PM_{2.5}$ resulted from a complex mix between local emissions and transported precursors from closer areas like the RRD. Indeed, pollutants from Southern China and the Red River Delta could still be brought to Hanoi via trajectories belonging to cluster C2. The winter means of $PM_{2.5}$ concentration (55.9 to 74.6 μg m^{-3}) were significantly higher during SC days compared to all the other types of days (Fig. 8). In particular, the rise of mean $PM_{2.5}$ level between SC and NEHA was approximately 24 - 29 μg m^{-3}. Finally, the OC days (strong wind from other directions than NE) mostly occurred during phase 3, out of the influence of cold surges with the appearance of trade winds originating from the ocean. Because these easterly air masses did not pass over any land before arriving to RRD, LRT will be negligible on these days. As the Northeast monsoon, the trade winds also enhanced the local wind speed, resulting in a considerable dilution of local pollution. However, the trade wind path covers the RRD region so that regional transport probably played a major role in the formation of $PM_{2.5}$ in Hanoi during OC days. Besides, high humidity conditions in this phase were favorable for the formation of secondary aerosols by heterogeneous reactions and their hygroscopic growth in ambient air. As a result, Figure 8 shows that the mean of $PM_{2.5}$ concentrations in OC days and NEHA had no significant difference and were even higher than in NELA itself.

4. Discussion

This study is not the first to use AOD data to track air pollution changes over the RRD plain. The high values of AOD across the RRD plain confirmed in this investigation are in agreement with earlier studies (Bui et al., 2021; Luong et al., 2021). Our findings highlight the AOD increase may be associated with the growing number of coal-based TPPs over the RRD plain between 2011 and 2020. Besides, a relation between the change of AOD in Hanoi and semi-climatic oscillations during the winter was revealed in a long-term analysis. During El Niño phases of the southern oscillation, the Northeast monsoon impact was found to be reduced and

478 western air masses became more frequent, leading to an increase of the smoke AOD from fires in
479 the western Indochina Peninsula and northern India, and a relative decrease of sulfate AOD
480 provided by LRT from China and regional transport from the RRD.

481 Regarding short-term variability, the results in this study seem to be different compared to
482 the previous study by Hien et al., 2011. However, the difference comes from the definition of
483 cold surges: Hien et al. (2011) defined cold surges only as the onset of cold intrusions (i.e. phase
484 1 only) while in this study, the term "cold surge" gathers the onset and prolongation of the cold
485 intrusions (phase 1 and 2). Generally, the results from both studies indicate a similar behavior in
486 which the ground-based $PM_{2.5}$ concentration drops significantly with the arrival of a cold
487 intrusion, then reaches its maximum level in the middle of the Northeast monsoon circulation.
488 This drop of surface $PM_{2.5}$ is mainly attributed to the dispersion of local pollution dominated by
489 the higher wind accompanying the cold surge onset, though it is difficult to quantify precisely the
490 rate of dilution.

491 The mean $PM_{2.5}$ concentration was higher by about 30 % or about 9 to 17 $\mu g.m^{-3}$ on NE-wind
492 high-AOD (NEHA) days compared to NE-wind low-AOD (NELA) days. This concentration
493 difference between NEHA and NELA days can be considered to represent the contribution of LRT
494 from mainland China. Of course, the exact value of $PM_{2.5}$ concentration increase that we obtained
495 depends on the threshold of Sulfate AOD that was chosen. However, one can note that this result is
496 very close from the 27% of LRT contribution that Hai and Kim Oanh, 2013 found using elemental
497 analysis on aerosol filter sampling. Indeed, when the monsoon air mass did not actually catch
498 pollution from China, which resulted in a lower sulfate AOD value, the observed $PM_{2.5}$
499 concentration represented only the local pollution and regional transport contributions. Conversely,
500 when the monsoon air mass did transport the Chinese plume to Hanoi, the $PM_{2.5}$ concentration
501 cumulated the local pollution and regional transport, plus the LRT contribution, which also
502 resulted in a higher sulfate AOD value. Following this reasoning, LRT from China represents a
503 significant, but minor part of the $PM_{2.5}$ level observed in Hanoi under the Northeast monsoon
504 impact. Our analysis is that, as the higher winds associated with the cold surge onset disperse the
505 local emissions, regional transport is possibly the dominant cause of air pollution in Hanoi under
506 the impact of the Northeast monsoon. Moreover, the role of regional transport was also proven
507 during the trade wind episodes (OC days), when the local wind is also enhanced, resulting in the
508 considerable dilution of local pollution. As the contribution of LRT is negligible when air masses

509 come from the ocean, regional transport combined with high humidity conditions are the main
510 factors enhancing the formation of $PM_{2.5}$ in Hanoi during OC days (phase 3).

511 During the middle of a monsoon episode (phase 2), the stagnant conditions (SC) make that
512 local pollution, plus pollutants from regional transport and LRT brought during the onset of the
513 cold surge, all remains trapped in Hanoi boundary layer. The air quality is further worsened as the
514 air subsidence associated with the anti-cyclone limits the boundary layer growth, resulting in the
515 most severe pollution episodes. The difference of average $PM_{2.5}$ concentrations between SC and
516 NEHA days can be interpreted as the contribution of local pollution, from 33 to 46 % or about 24
517 to 29 $\mu g.m^{-3}$. This result is lower than the range of values obtained by Nguyen et al., 2020 using
518 the WRF/CMAQ model (42 to 57% of local pollution contribution) but their study concerned only
519 the month of December 2010, during which a strong El Niño episode was ongoing. Consequently,
520 there was likely a lesser contribution of LRT from China during this month, which in return
521 increased the share of local pollution. To sum up, the local pollution and regional transport within
522 Northern Vietnam are found to contribute by a large part in the fine particle pollution in Hanoi.
523 LRT from China is taken into account but only contributes in a minor part to these polluted
524 episodes.

525 **5. Summary**

526 This study combined a long-term dataset of AOD from the NAAPS model with back-
527 trajectory clustering using the HYSPLIT model. During the first 5 winters (2006/07 to 2010/11),
528 the highest AOD values were observed over the Indochina Peninsula region, and this was mainly
529 due to anthropogenic and natural biomass burning. For the rest of the studied period, the AOD
530 map series indicated a very sharp increase in eastern China and northern Vietnam (the RRD
531 plain) following the rapid economic development of the area. Although this increasing trend
532 broke off during the last three winters of the study (from 2017/18 to 2019/20), the AOD in Hanoi
533 remained high. As a result, the major source of particles in Hanoi shifted from biomass burning
534 until 2011, to industrial activities for the rest of the studied period.

535 During El Niño events (winters 2014/15, 2015/16 and 2018/19), the share of northeastern
536 clusters, that correspond to the monsoon air masses, clearly decreased while western clusters were
537 more frequent. This was associated with a temporary decrease of the sulfate partial AOD, and to a
538 lesser extent, with an increase of the smoke partial AOD. Following the sources identified in the

first part of the study, this result was expected as northeastern air masses transiting over mainland China as well as Red River Delta are more susceptible to carry industrial pollution over Hanoi; conversely, western air masses from the Indochina Peninsula and Northern India are more likely to bring biomass burning aerosols over Hanoi. As a result, the change in air mass origin resulted in changes of the aerosol load and of the type of aerosols in Hanoi.

At last, in order to determine the contributions of the local, regional and transboundary sources of particles, a classification of the winter days was developed, combining meteorological features (wind speed and direction) with sulfate AOD, and this classification was applied to the four last winters (from 2016/17 to 2019/20). The discrepancy in the average level of $PM_{2.5}$ between the different types of days allowed to estimate the contribution of transboundary LRT from mainland China to be around 30 %. Transboundary LRT from mainland China is thereby not the dominant contributor to Hanoi's air pollution; instead, the regional transport may be the main contributor to air pollution in Hanoi under the impact of the Northeast monsoon. During the stagnant condition days, the estimated fraction of local pollution was about 40 %. As the contribution of transboundary LRT can be neglected during these days, the regional transport from the RRD thus also contributed to a large extent to the fine particle pollution in Hanoi in this case.

In the future, the source apportionment could be improved using observations from an Aerosol Chemical Speciation Monitor (ACSM) bringing information on $PM_{2.5}$ chemical composition. As the monsoon cycle phases are associated with different boundary layer depth values, it would also be interesting to discriminate the effects of pollution advection and vertical dilution, which could be done using lidar or ceilometer boundary layer depth observations.

Acknowledgments

The authors sincerely acknowledge the CPER (Contrat de Plan Etat-Région) research project IRenE (Innovation et Recherche en Environnement) and Climibio. The work is supported by the French Ministère de l'Enseignement Supérieur, de la Recherche et de l'Innovation, the region Hauts-de-France and the European Regional Development Fund. The work is also supported by the CaPPA project. The CaPPA project (Chemical and Physical Properties of the Atmosphere) is funded by the French National Research Agency (ANR) through the PIA (Programme d'Investissement d'Avenir; contract no. ANR-11-LABX-0005-01) and by the regional council of Nord-Pas-de-Calais and the European Regional Development Fund. The regional online databases

of pollutants and meteorology provided by different websites are genuinely appreciated, especially the $PM_{2.5}$ database from Environmental Protection Agency (EPA).

References

Ashfold, M.J., Latif, M.T., Samah, A.A., Mead, M.I., Harris, N.R.P., 2017. Influence of Northeast Monsoon cold surges on air quality in Southeast Asia. Atmospheric Environment 166, 498–509. https://doi.org/10.1016/j.atmosenv.2017.07.047

Bac, V.T., Hien, P.D., 2009. Regional and local emissions in red river delta, Northern Vietnam. Air Qual Atmos Health 2, 157–167. https://doi.org/10.1007/s11869-009-0042-2

Bui, T.H., Nguyen, D.L., Nguyen, H.H., 2021. Study of aerosol optical properties at two urban areas in the north of Vietnam with the implication for biomass burning impacts. Environ Sci Pollut Res. https://doi.org/10.1007/s11356-021-15608-5

Cabello, M., Orza, J.A.G., Galiano, V., Ruiz, G., 2008. Influence of meteorological input data on backtrajectory cluster analysis - a seven year study for southeastern Spain. Adv. Sci. Res. 2, 65–70. https://doi.org/10.5194/asr-2-65-2008

Chang, L., Xu, J., Tie, X., Wu, J., 2016. Impact of the 2015 El Nino event on winter air quality in China. Sci Rep 6, 34275. https://doi.org/10.1038/srep34275

Chen, T.-C., Yen, M.-C., Huang, W.-R., Jr, W.A.G., 2002. An East Asian Cold Surge: Case Study. Monthly Weather Review 130, 20. https://doi.org/10.1175/1520-0493(2002)130<2271:AEACSC>2.0.CO;2

Chen, T.-F., Chang, K.-H., Tsai, C.-Y., 2014. Modeling direct and indirect effect of long range transport on atmospheric $PM_{2.5}$ levels. Atmospheric Environment 89, 1–9. https://doi.org/10.1016/j.atmosenv.2014.01.065

Chew, B.N., Campbell, J.R., Hyer, E.J., Salinas, S.V., Reid, J.S., Welton, E.J., Holben, B.N., Liew, S.C., 2016. Relationship between aerosol optical depth and particulate matter over Singapore: Effects of aerosol vertical distributions. Aerosol Air Qual Res 16, 2818–2830. https://doi.org/10.4209/aaqr.2015.07.0457

Chuang, M.-T., Lee, C.-T., Hsu, H.-C., 2018. Quantifying $PM_{2.5}$ from long-range transport and local pollution in Taiwan during winter monsoon: An efficient estimation method. Journal of Environmental Management 227, 10–22. https://doi.org/10.1016/j.jenvman.2018.08.066

Co, H.X., Dung, N.T., Oanh, N.T.K., Hang, N.T., Phuc, N.H., Le, H.A., 2014. Levels and Composition of Ambient Particulate Matter at a Mountainous Rural Site in Northern Vietnam. Aerosol Air Qual. Res. 14, 1917–1928. https://doi.org/10.4209/aaqr.2013.09.0300

603 Cohen, D.D., Crawford, J., Stelcer, E., Bac, V.T., 2010a. Characterisation and source
604 apportionment of fine particulate sources at Hanoi from 2001 to 2008. Atmospheric
605 Environment 44, 320–328. https://doi.org/10.1016/j.atmosenv.2009.10.037

606 Cohen, D.D., Crawford, J., Stelcer, E., Bac, V.T., 2010b. Long range transport of fine particle
607 windblown soils and coal fired power station emissions into Hanoi between 2001 to 2008.
608 Atmospheric Environment 44, 3761–3769. https://doi.org/10.1016/j.atmosenv.2010.06.047

609 Cui, R.Y., Hultman, N., Cui, D., McJeon, H., Yu, S., Edwards, M.R., Sen, A., Song, K.,
610 Bowman, C., Clarke, L., Kang, J., Lou, J., Yang, F., Yuan, J., Zhang, W., Zhu, M., 2021.
611 A plant-by-plant strategy for high-ambition coal power phaseout in China. Nat Commun
612 12, 1468. https://doi.org/10.1038/s41467-021-21786-0

613 Ding, A., Huang, X., Nie, W., Chi, X., Xu, Zheng, Zheng, L., Xu, Zhengning, Xie, Y., Qi, X.,
614 Shen, Y., Sun, P., Wang, J., Wang, L., Sun, J., Yang, X.-Q., Qin, W., Zhang, X., Cheng,
615 W., Liu, W., Fu, C., 2019. Significant reduction of PM 2.5 in eastern China due to
616 regional-scale emission control: evidence from SORPES in 2011–2018. Atmospheric
617 Chemistry and Physics 19, 11791–11801. https://doi.org/10.5194/acp-19-11791-2019

618 Draxler, R.R., Hess, G.D., 1998. An Overview of the HYSPLIT_4 Modelling System for
619 Trajectories, Dispersion, and Deposition. Australian Meteorological Magazine 47, 295–
620 308.

621 Huang, K., Fu, J.S., Hsu, N.C., Gao, Y., Dong, X., Tsay, S.-C., Lam, Y.F., 2013. Impact
622 assessment of biomass burning on air quality in Southeast and East Asia during BASE-
623 ASIA. Atmospheric Environment 78, 291–302.
624 https://doi.org/10.1016/j.atmosenv.2012.03.048

625 Huy, L.N., Kim Oanh, N.T., 2017. Assessment of national emissions of air pollutants and
626 climate forcers from thermal power plants and industrial activities in Vietnam.
627 Atmospheric Pollution Research 8, 503–513. https://doi.org/10.1016/j.apr.2016.12.007

628 Junker, C., Wang, J.-L., Lee, C.-T., 2009. Evaluation of the effect of long-range transport of air
629 pollutants on coastal atmospheric monitoring sites in and around Taiwan. Atmospheric
630 Environment 43, 3374–3384. https://doi.org/10.1016/j.atmosenv.2009.03.035

631 Kuerban, M., Waili, Y., Fan, F., Liu, Y., Qin, W., Dore, A.J., Peng, J., Xu, W., Zhang, F., 2020.
632 Spatio-temporal patterns of air pollution in China from 2015 to 2018 and implications for
633 health risks. Environmental Pollution 258, 113659.
634 https://doi.org/10.1016/j.envpol.2019.113659

635 Le, H.A., Phuong, D.M., Linh, L.T., 2020. Emission inventories of rice straw open burning in the
636 Red River Delta of Vietnam: Evaluation of the potential of satellite data. Environmental
637 Pollution 260, 113972. https://doi.org/10.1016/j.envpol.2020.113972

638 Le, N.H., Ly, B.-T., Thai, P.K., Pham, G.-H., Ngo, I.-H., Do, V.-N., Le, T.T., Nhu, L.V., Son,
639 H.D., Nguyen, Y.-L.T., Pham, D.H., Vu, T.V., 2021. Assessing the Impact of Traffic
640 Emissions on Fine Particulate Matter and Carbon Monoxide Levels in Hanoi through
641 COVID-19 Social Distancing Periods. Aerosol Air Qual. Res. 21, 210081.
642 https://doi.org/10.4209/aaqr.210081

643 Leng, C., Duan, J., Xu, C., Zhang, H., Wang, Yifan, Wang, Yanyu, Li, X., Kong, L., Tao, J.,
644 Zhang, R., Cheng, T., Zha, S., Yu, X., 2016. Insights into a historic severe haze event in
645 Shanghai: synoptic situation,boundary layer and pollutants. Atmos. Chem. Phys. 16,
646 9221–9234. https://doi.org/10.5194/acp-16-9221-2016

647 Li, J., 2020. Pollution Trends in China from 2000 to 2017: A Multi-Sensor View from Space.
648 Remote Sensing 12, 208. https://doi.org/10.3390/rs12020208

649 Luong, N.D., Hieu, B.T., Hiep, N.H., 2021. Contrasting seasonal pattern between ground-based
650 PM2.5 and MODIS satellite-based aerosol optical depth (AOD) at an urban site in Hanoi,
651 Vietnam. Environ Sci Pollut Res. https://doi.org/10.1007/s11356-021-16464-z

652 Ly, B.-T., Matsumi, Y., Vu, T.V., Sekiguchi, K., Nguyen, T.-T., Pham, C.-T., Nghiem, T.-D.,
653 Ngo, I.-H., Kurotsuchi, Y., Nguyen, T.-H., Nakayama, T., 2021. The effects of
654 meteorological conditions and long-range transport on PM2.5 levels in Hanoi revealed
655 from multi-site measurement using compact sensors and machine learning approach.
656 Journal of Aerosol Science 152, 105716. https://doi.org/10.1016/j.jaerosci.2020.105716

657 Maciszewska, A.E., Markowicz, K.M., Witek, M.L., 2010. A multiyear analysis of aerosol
658 optical thickness over Europe and Central Poland using NAAPS model simulation. Acta
659 Geophys. 58, 1147–1163. https://doi.org/10.2478/s11600-010-0034-5

660 Miao, Y., Liu, S., Guo, J., Huang, S., Yan, Y., Lou, M., 2018. Unraveling the relationships
661 between boundary layer height and PM2.5 pollution in China based on four-year
662 radiosonde measurements. Environmental Pollution 243, 1186–1195.
663 https://doi.org/10.1016/j.envpol.2018.09.070

664 Minh, T.C., 2007. An outline of climatology and meteorology. Vietnam National University
665 Press, Hanoi.

666 Nguyen, D.-L., Czech, H., Pieber, S.M., Schnelle-Kreis, J., Steinbacher, M., Orasche, J., Henne,
667 S., Popovicheva, O.B., Abbaszade, G., Engling, G., Bukowiecki, N., Nguyen, N.-A.,
668 Nguyen, X.-A., Zimmermann, R., 2021. Carbonaceous aerosol composition in air masses
669 influenced by large-scale biomass burning: a case study in northwestern Vietnam. Atmos.
670 Chem. Phys. 21, 8293–8312. https://doi.org/10.5194/acp-21-8293-2021

671 Phung Ngoc, B.-A., Delbarre, H., Deboudt, K., Dieudonné, E., Nguyen Tran, D., Le Thanh, S.,
672 Pelon, J., Ravetta, F., 2021. Key factors explaining severe air pollution episodes in Hanoi

during 2019 winter season. Atmospheric Pollution Research 12, 101068. https://doi.org/10.1016/j.apr.2021.101068

Pu, W., Zhao, X., Shi, X., Ma, Z., Zhang, X., Yu, B., 2015. Impact of long-range transport on aerosol properties at a regional background station in Northern China. Atmospheric Research 153, 489–499. https://doi.org/10.1016/j.atmosres.2014.10.010

Reid, J.S., Hyer, E.J., Johnson, R.S., Holben, B.N., Yokelson, R.J., Zhang, J., Campbell, J.R., Christopher, S.A., Di Girolamo, L., Giglio, L., Holz, R.E., Kearney, C., Miettinen, J., Reid, E.A., Turk, F.J., Wang, J., Xian, P., Zhao, G., Balasubramanian, R., Chew, B.N., Janjai, S., Lagrosas, N., Lestari, P., Lin, N.-H., Mahmud, M., Nguyen, A.X., Norris, B., Oanh, N.T.K., Oo, M., Salinas, S.V., Welton, E.J., Liew, S.C., 2013. Observing and understanding the Southeast Asian aerosol system by remote sensing: An initial review and analysis for the Seven Southeast Asian Studies (7SEAS) program. Atmospheric Research 122, 403–468. https://doi.org/10.1016/j.atmosres.2012.06.005

Stein, A.F., Draxler, R.R., Rolph, G.D., Stunder, B.J.B., Cohen, M.D., Ngan, F., 2015. NOAA's HYSPLIT Atmospheric Transport and Dispersion Modeling System. Bull. Amer. Meteor. Soc. 96, 2059–2077. https://doi.org/10.1175/BAMS-D-14-00110.1

Yuan, J., 2018. The future of coal in China. Resources, Conservation and Recycling 129, 290–292. https://doi.org/10.1016/j.resconrec.2016.12.006

Zhao, S., Zhang, H., Xie, B., 2018. The effects of El Niño–Southern Oscillation on the winter haze pollution of China. Atmos. Chem. Phys. 18, 1863–1877. https://doi.org/10.5194/acp-18-1863-2018

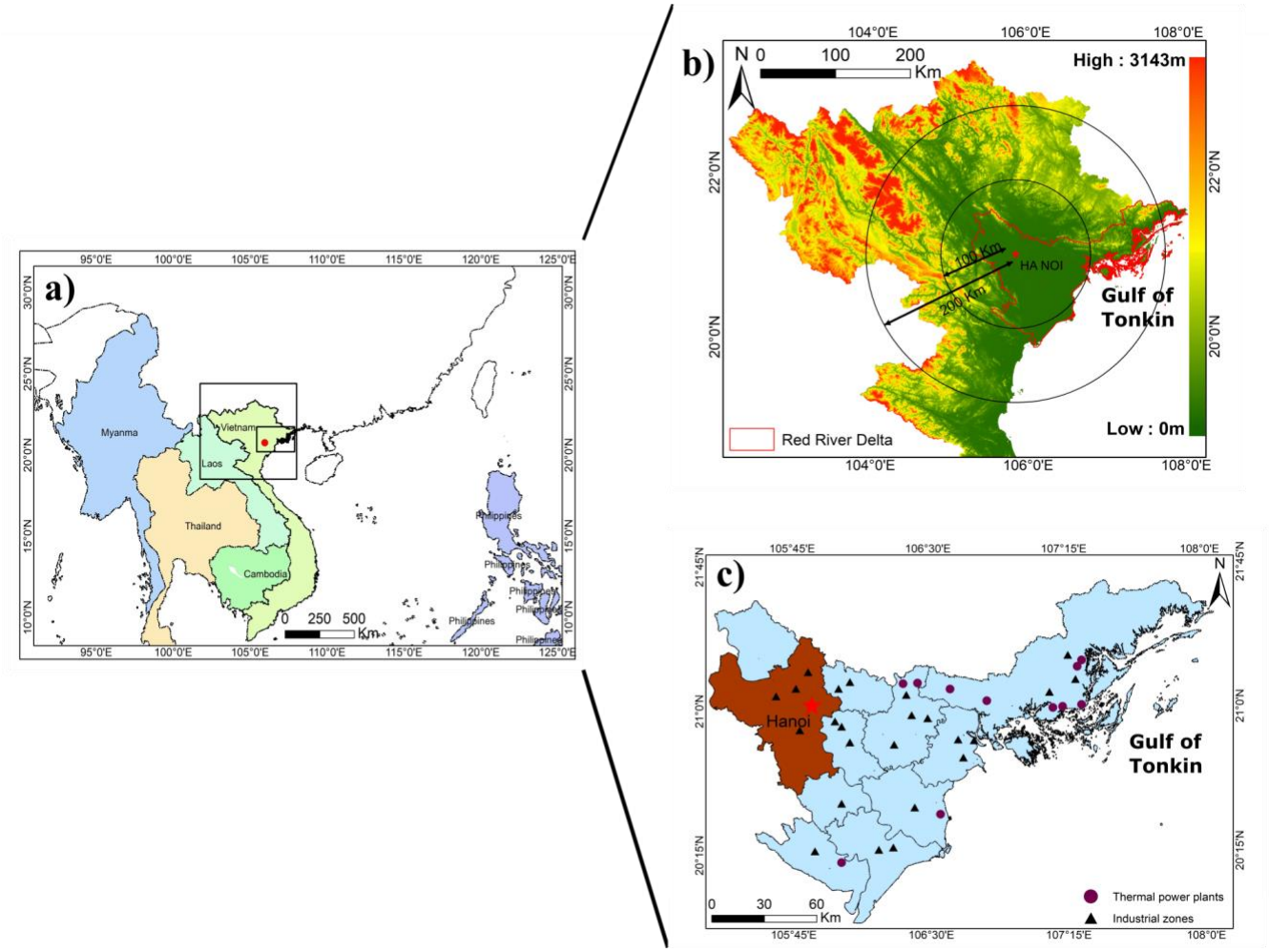

Figure 1. The geographical map of Vietnam and neighboring areas (a) showing the locations of the studied site in Hanoi (base map: ground altitude) (b) and industrial zones and thermal power plants over Red River Delta, Northern Vietnam (c). The outer circle with a 200 km radius in Figure 1(b) illustrates the distance threshold used to discriminate regional and long-range transport; it corresponds to the approximate distance from Hanoi to the Vietnam - China and Vietnam - Laos borders. The red star in Figure 1 (c) represents the city of Hanoi.

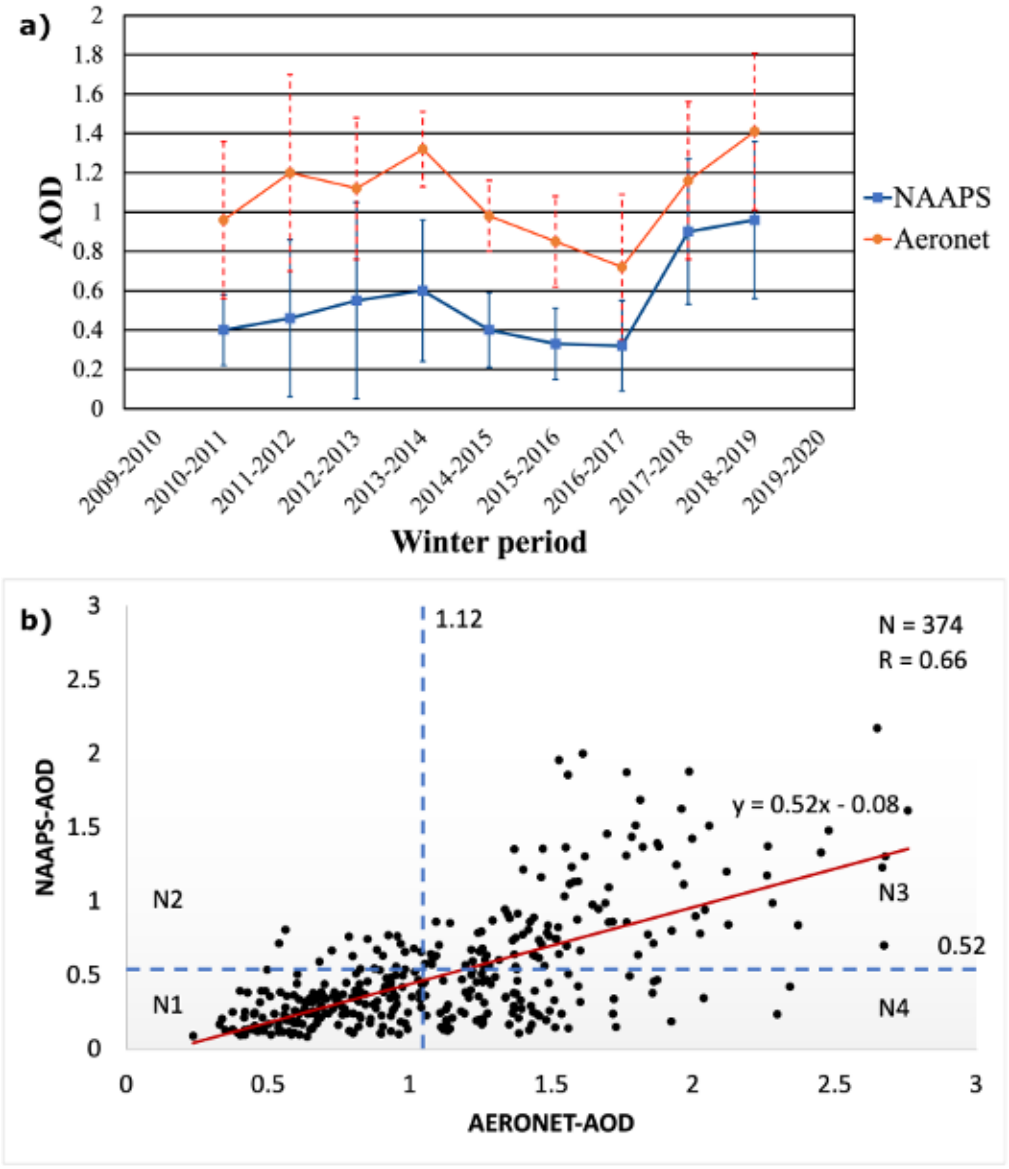

Figure 2. Comparison of the total AOD daily average values at 550 nm from the NAAPS model and at 500 nm from the Nghia-Do AERONET station: (a) 6-month winter averages from 2010/11 to 2018/2019 (the error bars represent the ±1σ standard deviation) and (b) point-to-point comparison. On panel (b), the plain red line represents the linear regression, while the blue dashed lines represent the all-point average AOD values. N is the total number of points included in the comparison, while N1 to N4 are the number of points falling in each quadrant. N1 = 168, N2 = 18, N3 = 105 and N4 = 83.

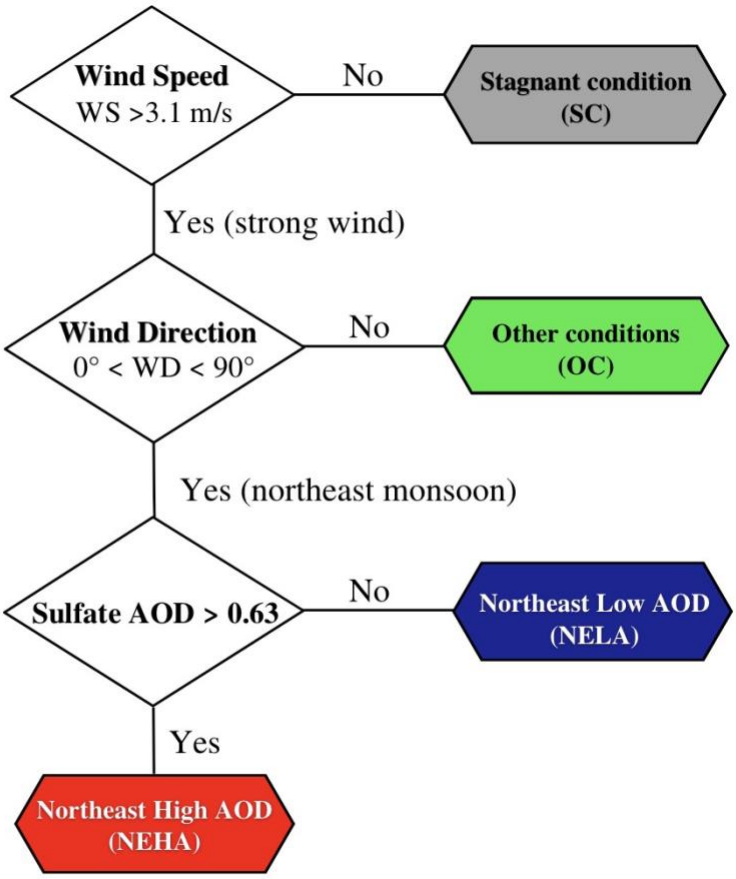

Figure 3. The schematic diagram of the classification of winter days. The winter days include “Stagnant conditions” - SC, “Northeast high AOD” - NEHA, "Northeast low AOD" - NELA and “Other conditions” – OC.

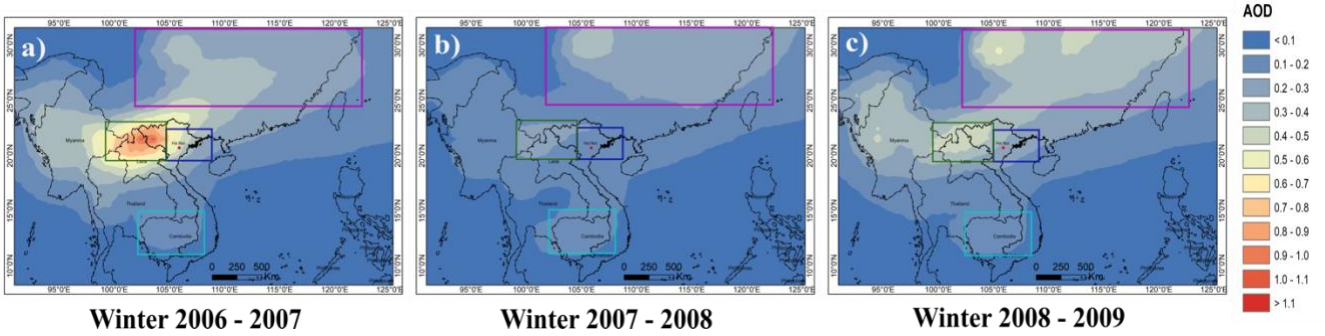

Winter 2006 - 2007 **Winter 2007 - 2008** **Winter 2008 - 2009**

(continued)

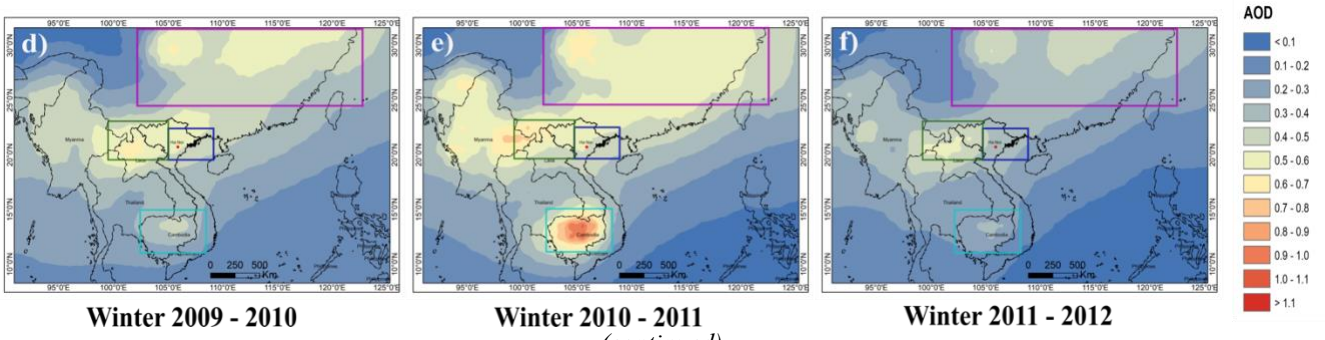

Winter 2009 - 2010 **Winter 2010 - 2011** **Winter 2011 - 2012**

(continued)

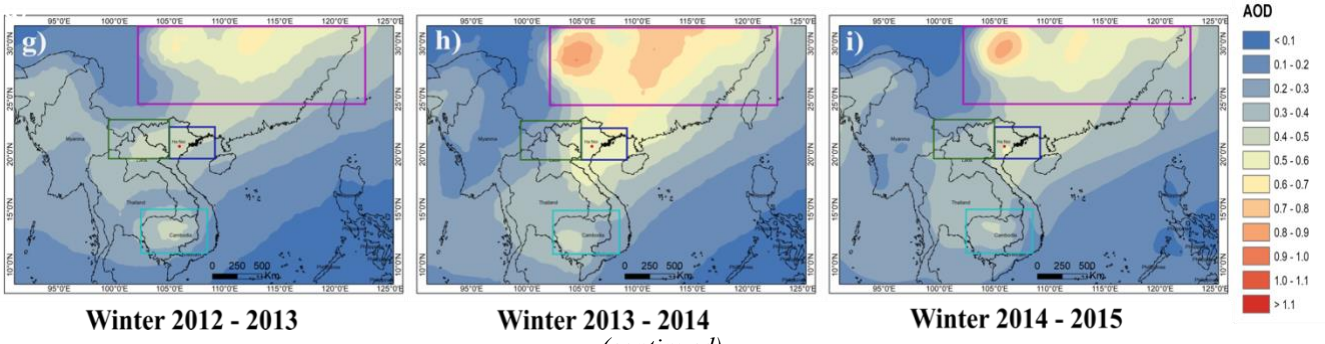

Winter 2012 - 2013 **Winter 2013 - 2014** **Winter 2014 - 2015**

(continued)

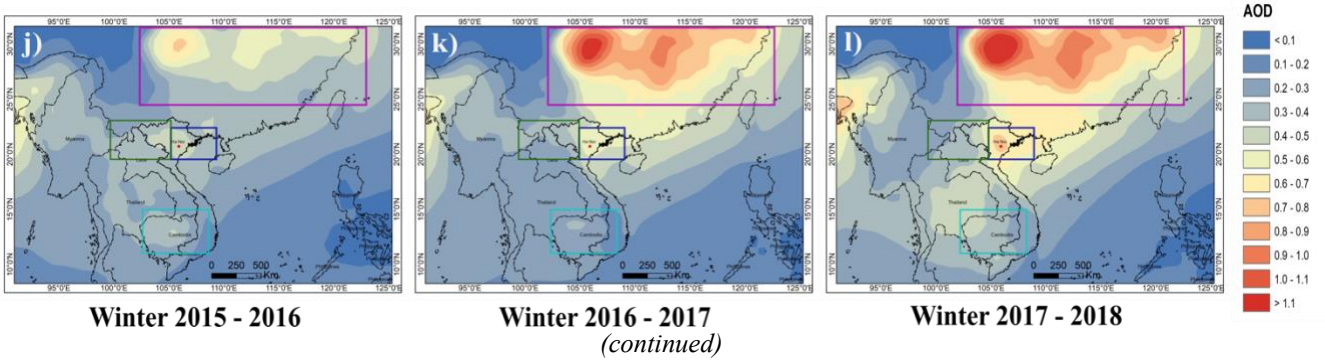

Winter 2015 - 2016 **Winter 2016 - 2017** **Winter 2017 - 2018**

(continued)

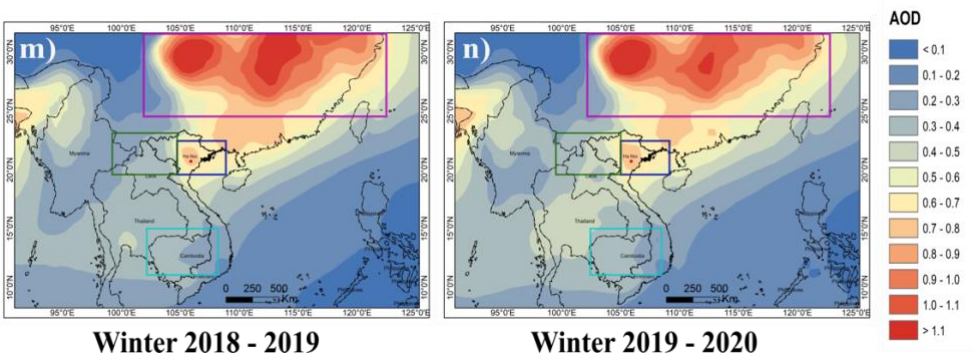

Figure 4. Time-averaged total AOD distribution during the winter periods from 2006/07 to 2019/20 (a – n) over Red River Delta, northern Vietnam (blue square) and the neighboring areas (mainland China - purple square, Indochina Peninsula region – green square and Cambodia – cyan square).

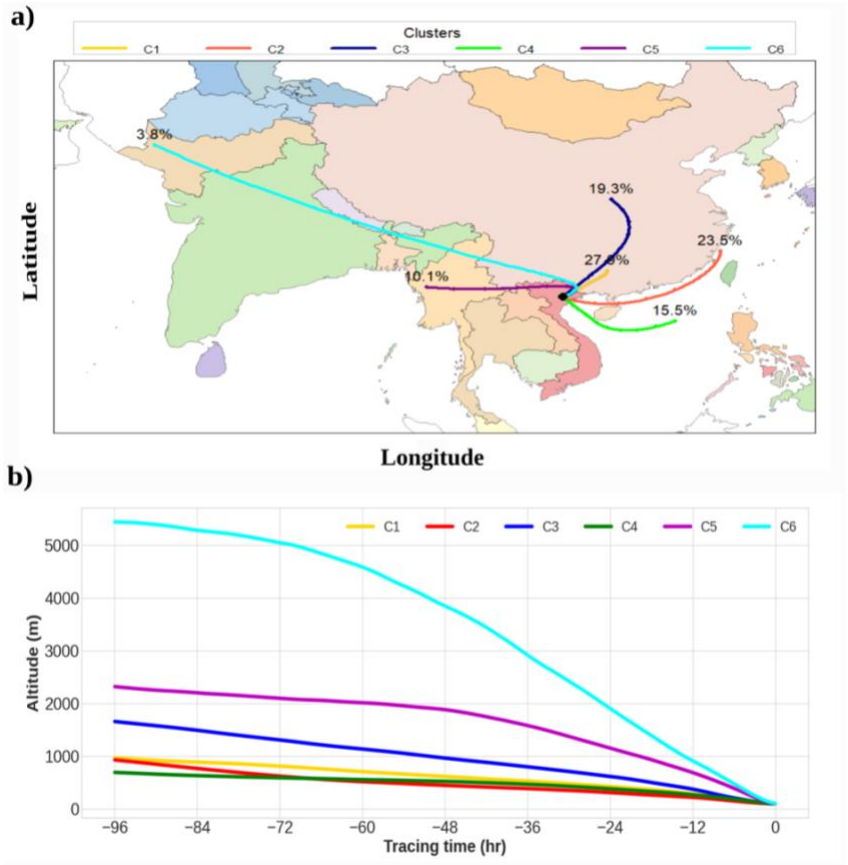

Figure 5. a) Mean 96-h backward air mass trajectories ending at Hanoi resulting from the clustering from October to March during the winter period of 2006-2020 and b) mean altitudes for each of these mean trajectories

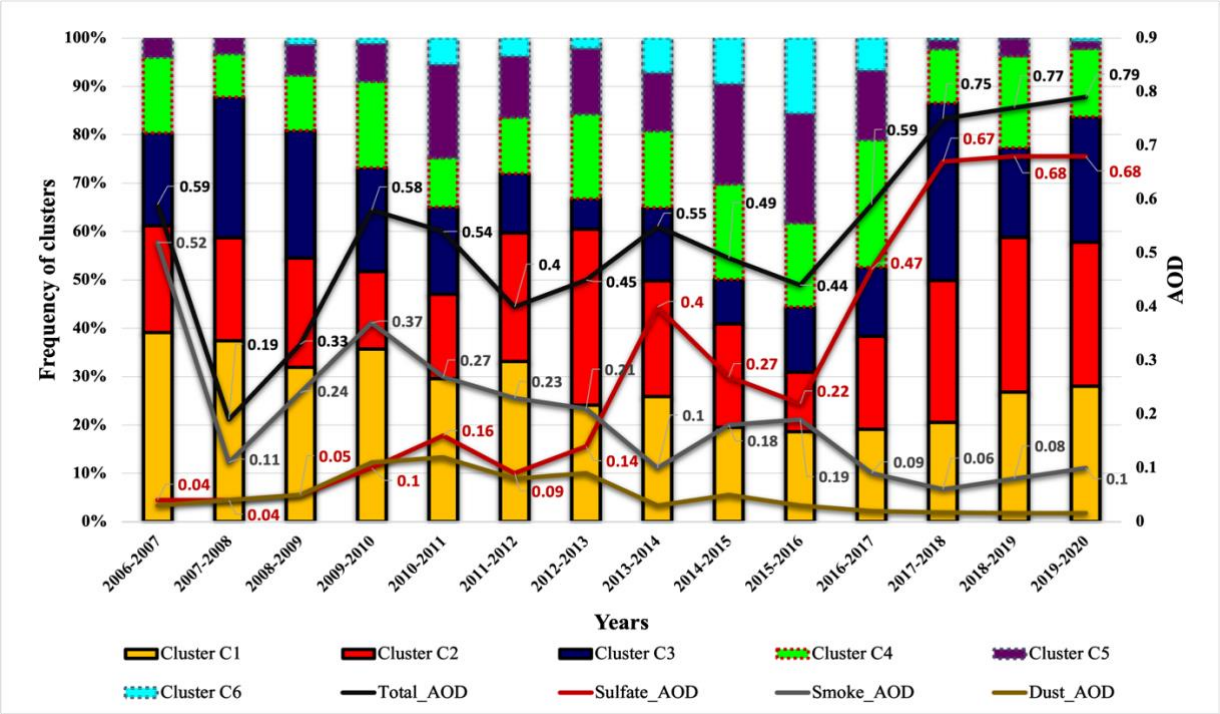

Figure 6. Frequency of occurrences for each cluster and variation of AOD over Hanoi during 14 winter seasons from period 2006/07 to period 2019/20.

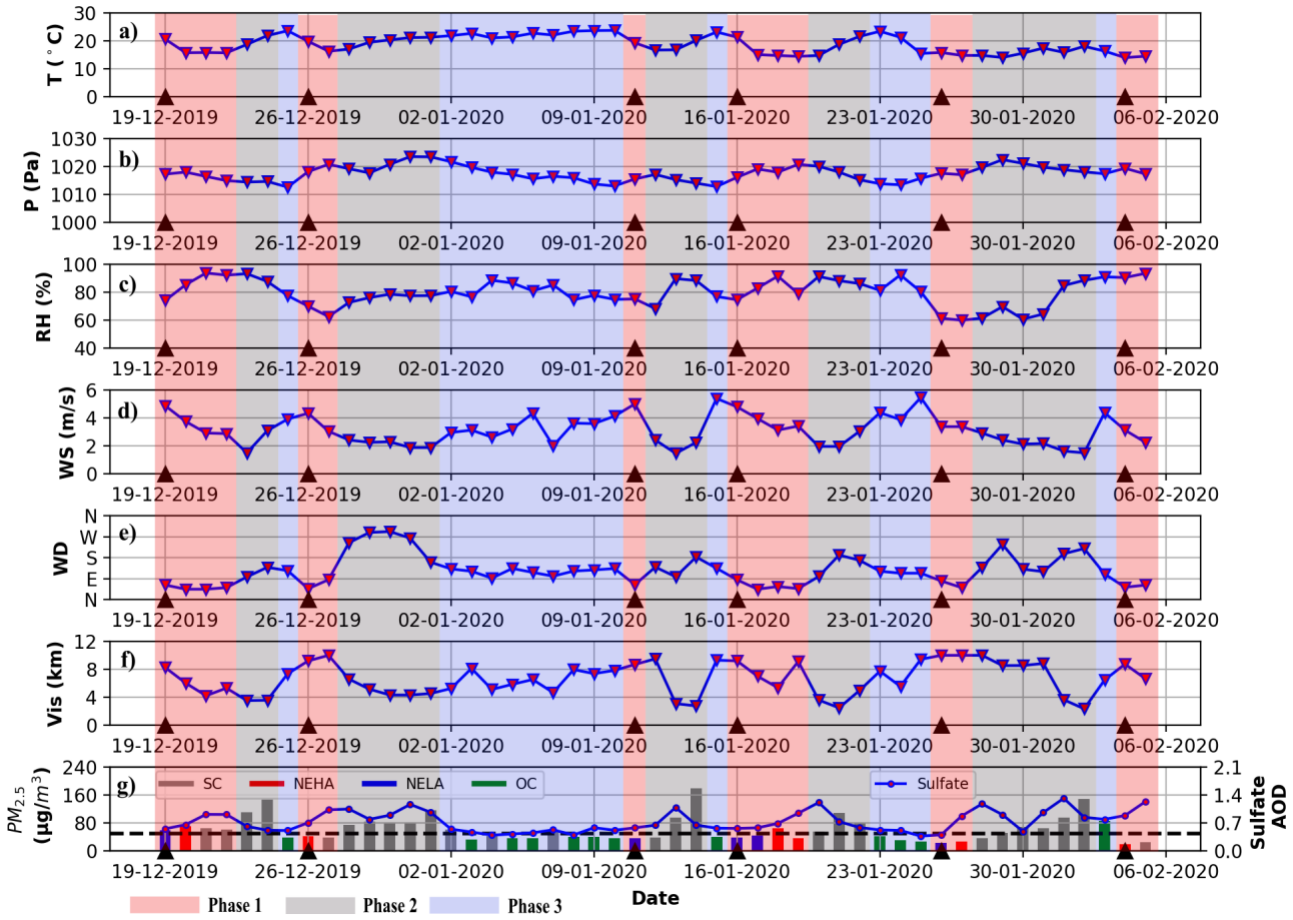

Figure 7. The daily average (a) temperature (T, ^{o}C), (b) pressure (P, Pa), (c) relative humidity (RH, %), (d) wind speed (WS, m/s), (e) wind direction (WD), (f) visibility (Vis, km), (g) $PM_{2.5}$ concentration (μg m^{-3}) and Sulfate AOD from 19th December 2019 to 05th February 2020. Black triangles on the horizontal axis mark the cold surges. The winter days include "Stagnant conditions" - SC, "Northeast high AOD" - NEHA, "Northeast low AOD" - NELA and "Other conditions" – OC. Phase 1, phase 2 and phase 3 were marked as red, grey and blue areas, respectively.

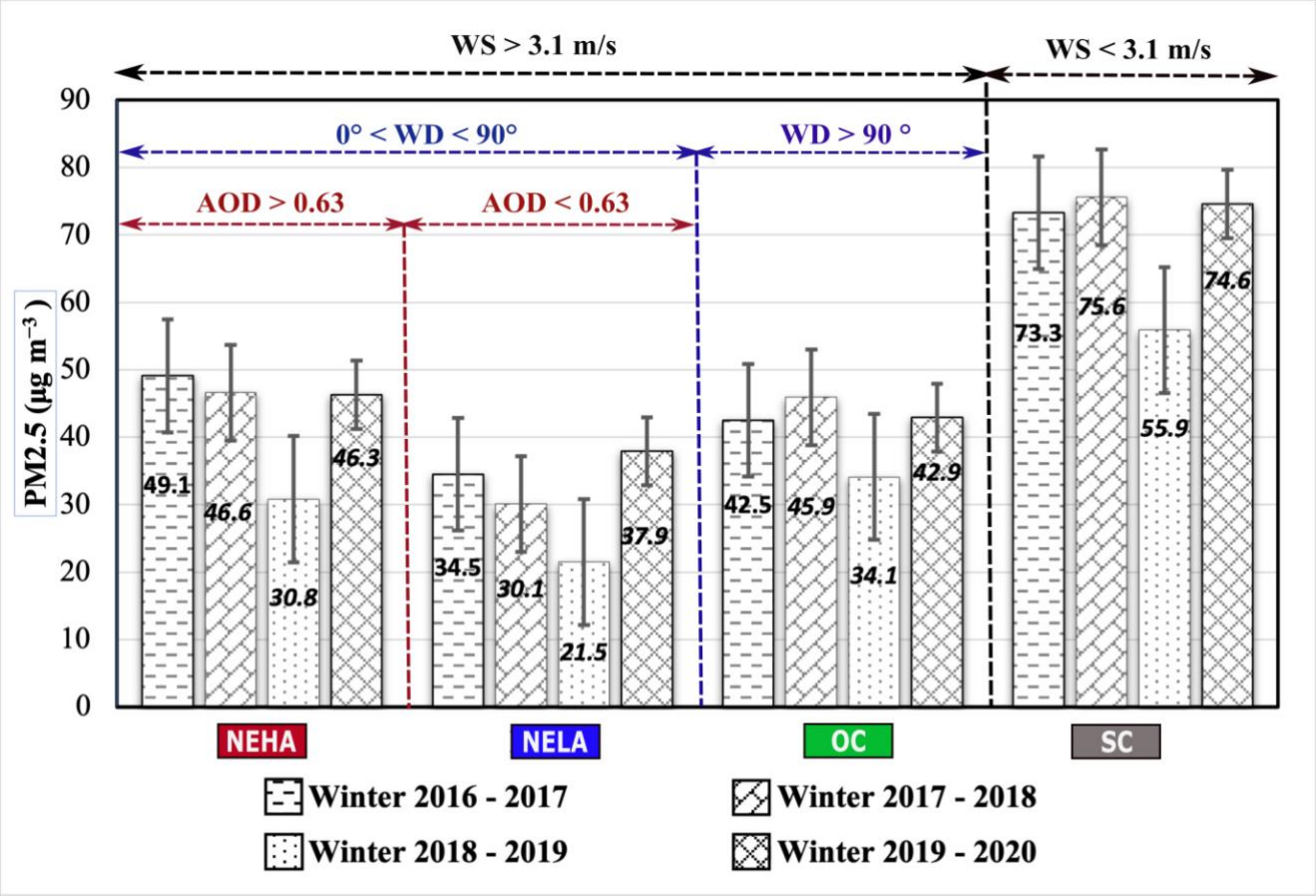

Figure 8. The averaged $PM_{2.5}$ concentration for the different types of winter days during the four winter periods (from period 2016/17 to period 2019/20). Error bars represent +/- 1 standard deviation of uncertainty.

Table

	Number of cold surges	Temperature (^{o}C)	Humidity (%)	Wind speed (m s^{-1})	Wind direction			Sulfate AOD
					Northeast (%)	Southeast (%)	Other (%)	
2016 - 2017	14	22.1 ± 4.0	74.9 ± 15.1	3.0 ± 0.9	27.4	51.1	21.5	0.46 ± 0.27
2017 - 2018	10	20.5 ± 4.1	73.4 ± 12.8	2.9 ± 0.8	26.1	56.2	17.7	0.64 ± 0.27
2018 - 2019	16	21.5 ± 4.1	80.6 ± 10.5	3.1 ± 0.9	34.6	54.9	10.5	0.65 ± 0.24
2019 - 2020	15	21.5 ± 3.6	76.9 ± 11.1	3 ± 0.9	29.7	51.9	18.4	0.65 ± 0.26
Average		21.3 ± 4.1	76.6 ± 12.7	3.1 ± 0.9	29.5	53.4	17.1	0.63 ± 0.28

Table 1: The mean and standard deviation of meteorological data and sulfate AOD data in each winter period from the winter period 2016/17 to period 2019/20.

	Averaged days per winter (days)	ΔWS (m/s)	ΔT (^{o}C)	ΔRH (%)	Δ$PM_{2.5}$ (μg m^{-3})	ΔSulfate AOD
Phase 1	~ 34	0.94 ± 0.68	-2.16 ± 3.03	-1.41 ± 13.05	-22.29 ± 18.31	0.02 ± 0.26
Phase 2	~ 87	-0.61 ± 0.45	-0.33 ± 2.59	-0.72 ± 12.21	13.32 ± 32.66	0.03 ± 0.25
Phase 3	~ 38	0.73 ± 0.54	2.34 ± 2.47	2.56 ± 10.25	-13.95 ± 19.27	-0.09 ± 0.19

Table 2: Mean and standard deviation of meteorological data, ground-based $PM_{2.5}$ and sulfate AOD in each phase during the 4-winter periods from 2016/17 to 2019/20. The mean and standard deviation are calculated after computing the delta between the actual values and the monthly average for each month of the 4-winter periods.

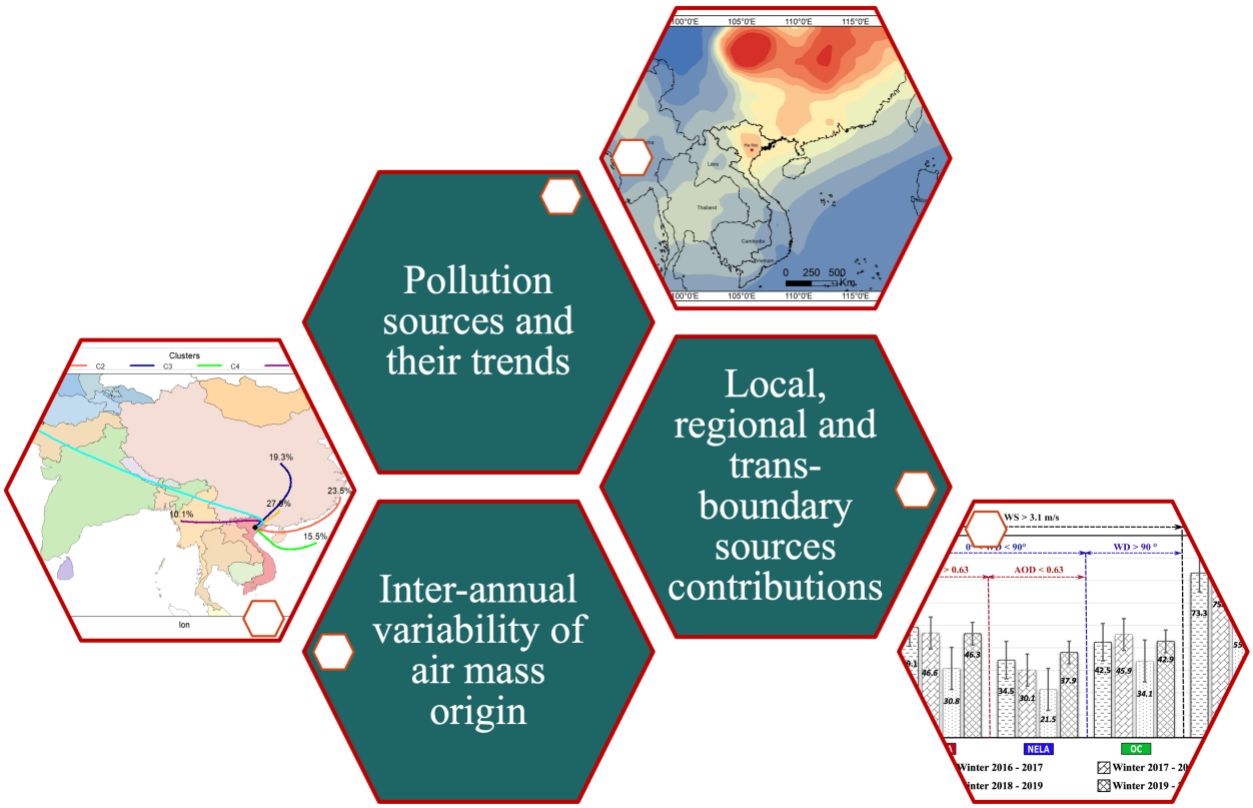
Pollution sources and their trends
Local, regional and trans-boundary sources contributions
Inter-annual variability of air mass origin
Clusters
C2
C3
C4
19.3%
27.6%
23.5%
10.1%
15.5%
lon
100°0'E
105°0'E
110°0'E
115°0'E
0 250 500 Km
WS > 3.1 m/s
WD > 90 °
AOD > 0.63
AOD < 0.63
NELA
OC
Winter 2016 - 2017
Winter 2017 - 20
Winter 2018 - 2019
Winter 2019 -